Dual Reversible Transformer Model for the Calculation of Low-Frequency Transients

Saeed Jazebi, *Student Member, IEEE*, Francisco de León, *Senior Member, IEEE*, Ashkan Farazmand, and Digvijay Deswal

***Abstract*—This paper presents a physically consistent dual model applicable to single-phase two-winding transformers for the calculation of low-frequency transients. First, the topology of a dual electrical equivalent circuit is obtained from the direct application of the principle of duality. Then, the model parameters are computed considering the variations of the transformer electromagnetic behavior under various operating conditions. Current modeling techniques use different topological models to represent diverse transient situations. The reversible model proposed in this paper unifies the terminal and topological equivalent circuits. The model remains invariable for all low-frequency transients including deep saturation conditions driven from any of the two windings. The proposed model is tested with a single-phase transformer for the calculation of magnetizing inrush currents, series ferroresonance, and geomagnetic-induced currents (GIC). The electromagnetic transient response of the model is compared to the π model and to laboratory measurements for validation.**

***Index Terms*—Electromagnetic transients, low-frequency transformer modeling, principle of duality, transformers.**

I. Introduction

TRANSFORMER models for transients are classified into several categories according to the frequency of the transient under study [1]–[3]. Inrush currents, ferroresonance, and geomagnetic-induced currents (GICs) are some of the most common low-frequency transients that are important for transformer studies and design. Inrush currents can be very large, in some cases exceeding 20 p.u., with long durations that may cause false tripping of differential protection, insulation degradation, and coil deformation due to mechanical stresses. Ferroresonance produces transients with short periods of high current and overvoltages on the windings, which may cause insulation failure. GICs are increasingly becoming a cause for concern since they can produce widespread blackouts.

A gamut of low-frequency transformer models exists in the literature [4]–[17]. Some models are valid for a very wide range of frequencies [4], [5]; some are specially developed for low-frequency transients [6]–[15]; and among them a few are specific for the calculation of inrush currents [12]–[17]. There are only a few models intended to compute ferroresonant overvoltages [8]. It has been established that the models derived from the principle of duality [18], best represent the transient phenomena in transformers [4]–[12]. This is so because each component in the model represents a physical region inside the transformer. However, different dual and physical models exist for the same transformer in the literature [1].

Other physically accurate models exist based on equivalent magnetic circuits; see [13] and [14]. However, these models are not dual electrical models and, therefore, they are not directly compatible with electromagnetic transient programs.

In 1991, Arturi highlighted a significant difference between the transient behavior of windings when the iron core goes into deep saturation [6]. He developed a time-domain dual model capable of simulating the out-of-phase synchronization condition. To correctly represent the heavily saturated behavior, linear inductances are connected in series with the magnetizing branches. Arturi's model is very detailed and relies on the availability of complete geometrical information of the iron core and windings. A similar approach is implemented in [8] to model a five-legged wound-core transformer for ferroresonance studies. Later, this method was expanded to develop a reversible transformer model in [14]. Reference [14] highlights the considerable difference between magnetizing inrush currents drawn from primary and secondary sides. The model in [14] is reversible and appropriate for the calculation of inrush currents of single-phase two-winding transformers. The model is derived from the solution of the magnetic equivalent circuit and, thus, is topologically correct. The only drawback of this model is that it cannot be built directly with circuit elements readily available in electromagnetic transient programs (EMTP type).

Existing guidelines propose the T model (with two leakage inductors, and one magnetizing branch) for the calculation of low-frequency transients [2], [3]. However, the T model is not physically consistent and there is evidence showing that it fails for transients involving deep saturation [19]–[22]. The weak behavior of the T model to predict inrush currents or ferroresonance has been reported in [21] and [22], respectively. The π model has been proposed as a more physical and accurate alternative [21]. In addition, the π model, with two magnetizing branches, provides more degrees of freedom to develop a dual reversible transformer model.

The main contribution of this paper is to propose a reversible model for single-phase two-winding transformers, obtained

Manuscript received April 02, 2013; accepted June 10, 2013. Date of publication July 09, 2013; date of current version September 19, 2013. Paper no. TPWRD-00376-2013.

S. Jazebi, F. de León, and A. Farazmand, are with the Department of Electrical and Computer Engineering, Polytechnic Institute of New York University, Brooklyn, NY, 11201 USA (e-mail: jazebi@ieee.org; fdeleon@poly.edu; farazmand@nyu.edu).

D. Deswal is with the Indian Institute of Technology, Kharagpur, West Bengal 721302, India (e-mail: deswal.digvijay@gmail.com).

Color versions of one or more of the figures in this paper are available online at http://ieeexplore.ieee.org.

Digital Object Identifier 10.1109/TPWRD.2013.2268857

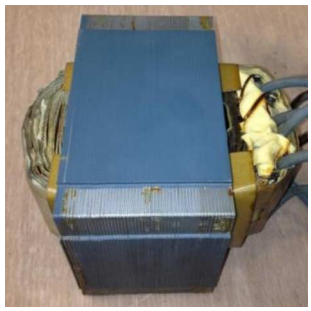

Fig. 1. Single-phase transformer with four windings.

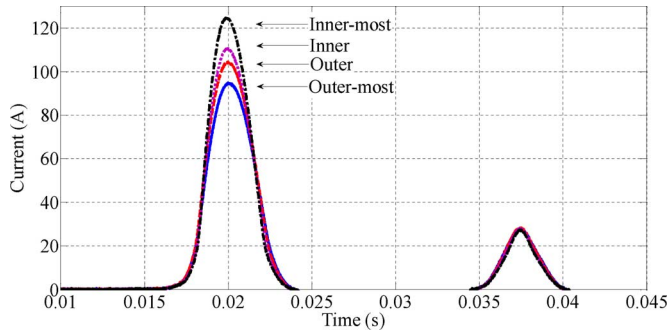

Fig. 2. Inrush currents measurements when energizing different windings at voltage zero crossing for the transformer of Fig. 1.

from the principle of duality, that properly represents the terminal behavior of transformers for low-frequency transients and including deep saturation conditions. The model presented in this paper joins the available circuit for transformers for the study of low-frequency transients. The model is self adaptive because with a unique set of parameters, it is capable of correctly describing the air-core inductance from both windings. This is an improvement over the π model of [21], where the air-core inductance needs to be changed to model energization from the high- or the low-voltage windings. In addition, the model can be built with circuit elements available in EMTP-type programs, which is a step forward from the model of [14].

Three-dimensional (3D) finite-element simulations are performed to study the behavior of the magnetic field in the transformer window. Nonlinear inductors are considered to account for the contribution of magnetic flux penetration in the air. These inductors are added to the structure of the π model between the windings and the transformer window. The model is useful for both transformer designers and power system analysts, because all circuit parameters can be measured at the terminals from tests, and no geometrical or material information is needed. EMTP simulation results are validated against measurements and 3D finite-element simulations for inrush currents, GIC, and ferroresonance studies.

II. Dual-Reversible Model

The conventional T equivalent circuit for two-winding transformers is valid for steady state conditions. The π circuit representation has been proven to be superior for transients involving deep saturation [21], [22]. However, the parameters of the π model need to be changed to provide sufficiently accurate results for transient studies on both windings.

A. Difference in the Transient Behavior of the Windings

From experience, it is known that different windings in transformers show different electromagnetic behavior in deep saturation [6], [14]. To illustrate the substantial difference between the transient behavior of different windings, inrush current switching experiments have been performed on the 1-kVA transformer shown in Fig. 1. This transformer has four separate layer-type windings with the same number of turns (108 turns); each winding has three layers with 36 turns. Complete transformer data are given in Appendix B.

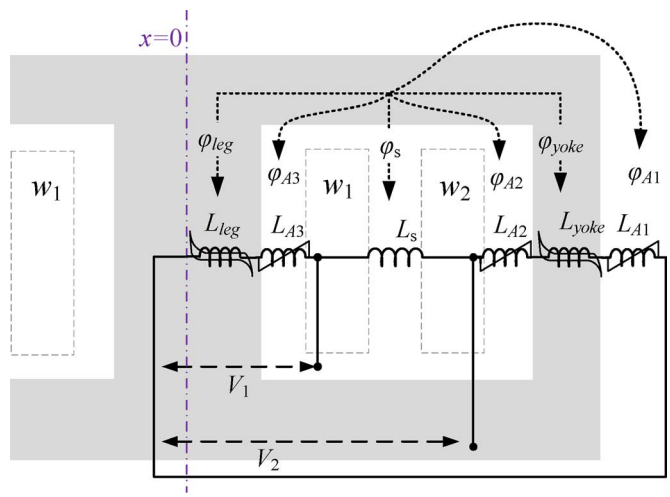

Fig. 3. Transformer model obtained from direct application of the principle of duality considering nonlinear inductors in air and hysteretic inductors for the core.

The experimental results presented in Fig. 2 show a significant difference in the magnitude of the first peak of inrush currents (31.5%) between the innermost and outermost windings, while the second peaks are almost the same. One can conclude that differences arise when the transformer is operating in deep saturation where the dominant factor is the corresponding air-core inductance of the windings [21], [22]. This difference could be higher for larger power transformers with larger inter-winding spacing, which contributes to the air-core inductance.

B. Modeling Principles

According to the principle of duality between electric and magnetic circuits, each flux path can be represented with an inductor (nonlinear hysteretic inductor for iron-core regions) [18]. The topology of the dual reversible model is derived from the direct application of the principle of duality between electric and magnetic circuits [11]; (see Fig. 3). This figure illustrates why the iron core needs to be divided into two parts in a duality-derived model. It also shows why the leakage inductance is unified. In fact, leakage inductance can only be defined (or measured) for a pair of windings during energy transfer [21]. The magnetizing inductance is divided into two parts: one part represents the leg plus half the yoke, and the other part represents half the yoke plus the returning leg.

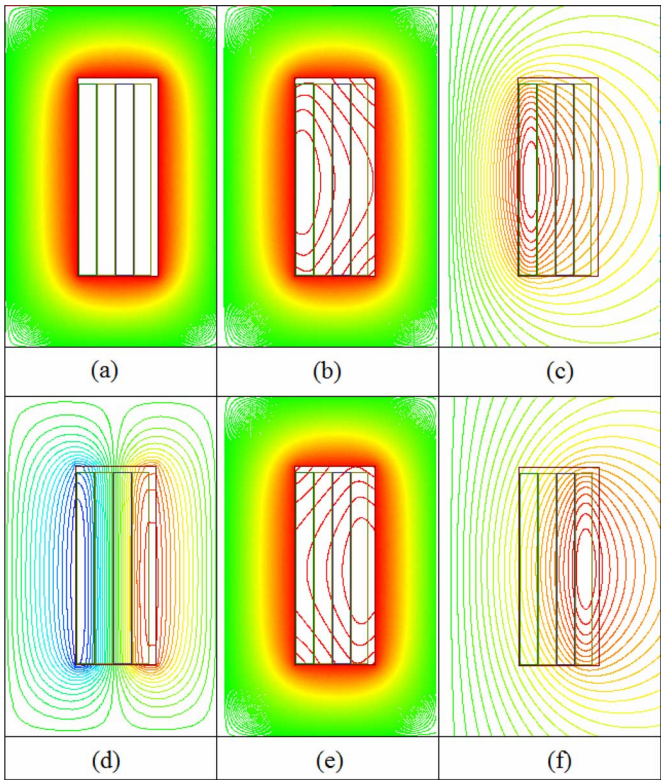

Fig. 4. Magnetic flux pattern extracted from FEM simulations in the right-half part of the transformer window for different operating conditions. (a) Open-circuit test, exciting from the innermost winding $\mu_r = 4000$. (b) Open-circuit test, exciting from the innermost winding $\mu_r = 50$. (c) Open-circuit test, exciting from the innermost winding $\mu_r = 1$. (d) Short circuit test between the innermost and outermost windings. (e) Open-circuit test, exciting from the outermost winding $\mu_r = 50$. (f) Open-circuit test, exciting from the outermost winding $\mu_r = 1$.

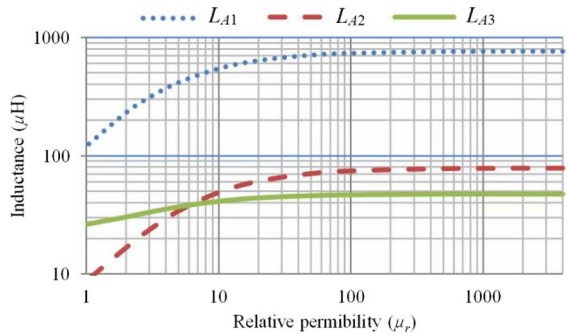

Fig. 5. Variation of the air inductance values with respect to the relative permeability of the iron core.

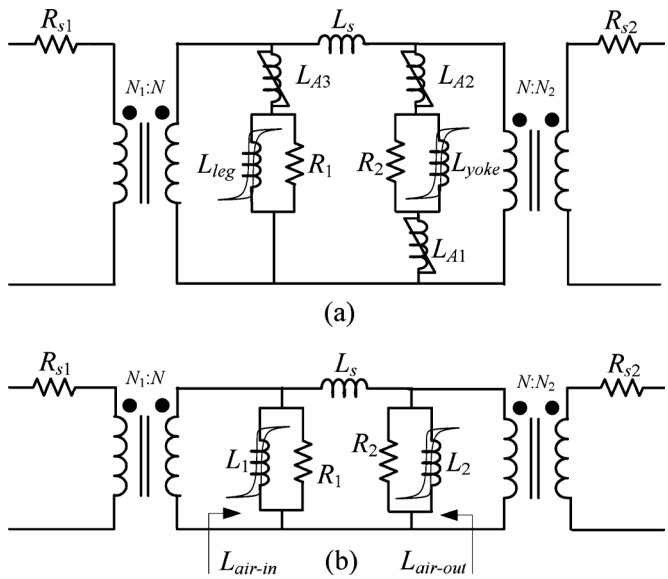

Fig. 6. Reversible transformer model. (a) Dual electrical equivalent circuit derived from Fig. 3. (b) Simplified reversible.π model.

Inductors L_{A1}, L_{A2}, and L_{A3} represent the magnetic field in the air (leakage and stray fields), outside and inside the transformer window. In this paper, different from previous publications, the inductors corresponding to magnetic energy in the air are considered to be nonlinear. When the iron core goes into saturation, its relative permeability gradually decreases. In deep saturation, the relative permeability tends to $\mu_r = 1$; therefore, saturated iron can be considered the same as air. This phenomenon, in addition to changing the behavior of the magnetic flux in the transformer core, affects the distribution pattern and magnitude of the magnetic flux in the air. Fig. 4 presents the patterns of the magnetic flux simulated with the finite-elements method in the air and core for different operating conditions. This figure shows how the changes in the electromagnetic behavior of the core are reflected in the distribution of the magnetic flux in air.

Fig. 5 shows the nonlinear behavior of the inductances corresponding to the magnetic energy in the air. The values are computed from the magnetic energy in the corresponding regions of the air (see Fig. 3) using FEM simulations. It is clear that air inductances change with the relative permeability of the iron core. It can be seen from Fig. 5 that the values of inductances in air remain relatively constant except when the core goes into saturation ($\mu_r < 100$). From the results presented in Figs. 4 and 5, one can see why the circuit parameter values of the dual model corresponding to open circuit, short circuit, and deep saturation should be different. The techniques that will be presented in this paper unify all equivalent circuits for low-frequency transients by considering the nonlinear behavior of the magnetic energy in the air caused by the saturation of the core.

The model of Fig. 3 can be rearranged to the electrical form of Fig. 6(a). The winding resistances R_{s1}, R_{s2} are added into the terminals of the ideal transformers. The constant resistors in parallel with hysteretic inductors only represent the eddy current losses in the core. This is a valid model according to the IEEE Task Force on Modeling and Analysis Guidelines for Slow Transients [3]. In addition, experiments confirm that eddy current losses in the windings can be represented adequately by a constant resistor for thin wires (less than 3-mm thickness) under low frequencies [23]. The losses due to hysteresis are fully modeled (including minor loops) by the hysteretic inductors in the EMTP-RV software.

Note that air inductances L_{A1}, L_{A2}, and L_{A3} are negligible during open circuit, short circuit, and normal operating conditions because the magnetic energy is concentrated in the iron core (magnetizing inductances) and between the windings (leakage inductance). However, in deep saturation, the value of the air inductances becomes comparable with the leakage

and magnetizing inductances. Therefore, air inductances can be presented by linear piece-wise approximations with two sections: 1) zero in normal conditions and 2) a constant slope line in deep saturation (corresponding to the permeability of air and winding geometry). The values of R_1 and R_2 in Fig. 6(a) are much larger than the corresponding impedances of L_{A1}, L_{A2}, L_{A3}, L_{leg}, and $L_{\rm yoke}$. Therefore, $L_{\rm leg}$ and L_{A3} are unified to a single inductor L_1. Also, $L_{\rm yoke}$, L_{A1}, and L_{A2} are unified to another equivalent inductor L_2. Finally, the model of Fig. 6(a) is simplified to the π model of Fig. 6(b). However, from the aforementioned explanations, the difference between this (reversible) model and the conventional π model is in deep saturation. In the new reversible model, the deep saturation inductances of the two magnetizing branches $L_{1-\rm sat}$, and $L_{2-\rm sat}$ are not the same as in the π model.

C. Calculation of Parameters

Geometrical dimensions or design information for transformers are almost never available to transformer customers. Therefore, it is essential to obtain parameter values of the model from terminal measurements.

Magnetizing branch parameters and leakage inductance are measured with the procedures proposed by the IEEE Standard C57.12.91-1995 for open-circuit and impedance tests.

In the open-circuit test, the low-voltage (LV) winding is energized, and the high-voltage (HV) winding is open circuited. The current of primary (low voltage) as well as secondary voltage (high voltage side) is recorded. The voltage values are referred to the primary side with the turns ratio. With modern instrumentation, it is possible to obtain time-domain samples of the open-circuit induced voltage. Therefore, the λ-i characteristic can be computed by integration over the induced voltage. In this paper, the trapezoidal rule of integration is used as follows:

$$\lambda(i) = \lambda(i-1) - \frac{V(i-1)+V(i)}{2}\Delta t \tag{1}$$

where λ is the linkage flux, V is the secondary voltage, and Δt is the time step. This information for each magnetizing branch of Fig. 6(b) is presented in Appendix B. Note that since there are two parallel magnetizing branches in the model, the measured values of the flux are kept constant, but the measured current values are multiplied by the factor of 0.5 [21].

To measure the leakage inductance and the winding resistances, the HV winding is energized while the LV winding is short circuited. The applied voltage is varied gradually to obtain the nominal current in the LV winding. The *rms* value of the terminal voltage $(V_{\rm sc})$, *rms* current $(I_{\rm sc})$, and active power $(P_{\rm sc})$ on the HV side are measured. DC resistance tests are also performed on the primary and secondary windings. The ac resistance obtained by the short-circuit test is divided into two components proportional to the dc resistances [21]. Therefore, impedance parameters are calculated with the following equations:

$$\begin{aligned} R_{s1} &= \frac{P_{\rm sc}}{I_{\rm sc}^2}\frac{R_{\rm dc1}}{R_{\rm dc1}+R_{\rm dc2}} \\ R'_{s2} &= \frac{P_{\rm sc}}{I_{sc}^2}\frac{R_{\rm dc2}}{R_{\rm dc1}+R_{\rm dc2}} \end{aligned} \tag{2}$$

$$L_s = \frac{1}{\omega_s}\sqrt{\left(\frac{V_{\rm sc}}{I_{\rm sc}}\right)^2 - \left(\frac{P_{\rm sc}}{I_{\rm sc}^2}\right)^2} \tag{3}$$

$$R_1 = R_2 = 2\frac{(V_{\rm oc}-R_{s1}I_{\rm oc})^2}{P_{\rm oc}} \tag{4}$$

where ω_s is the angular frequency, and R'_{s2} is the ac resistance of the secondary winding referred to the primary winding. Parameters $V_{\rm oc}$, $I_{\rm oc}$, and $P_{\rm oc}$ are the open circuit rms voltage, rms current, and active power measured on the primary side, respectively.

Hybrid *ac-dc* laboratory tests were performed to measure the air-core inductances of the HV and LV windings [24]. A low-power static uncontrolled rectifier with ripple is connected to the primary winding, with the secondary winding open-circuited. The primary ac current and the secondary ac voltage are measured. To extract the amplitude of the fundamental voltage and current, Fourier transform is applied. Then, the air-core inductance is obtained with the following expression:

$$L_{\rm air} = \frac{V_{2f}}{2\pi f\, n\, I_{1f}} \tag{5}$$

where $L_{\rm air}$ is the air-core inductance seen from the excited winding, n is the turns ratio, f is the nominal frequency V_{2f} is the amplitude of the secondary fundamental voltage, and I_{1f} is the amplitude of the primary fundamental current. This test is performed on the LV and HV windings to obtain $L_{\rm air-in}$, and $L_{\rm air-out}$. A complete description of the air-core inductance measurement procedure is available in [24].

The equivalent air-core inductances from the inner and outer windings of the model presented in Fig. 6(b) could be calculated by neglecting all damping components as follows:

$$L_{\rm air-in} = \frac{L_{1-\rm sat}(L_s+L_{2-\rm sat})}{L_{1-\rm sat}+L_{2-\rm sat}+L_s} \tag{6}$$

$$L_{\rm air-out} = \frac{L_{2-\rm sat}(L_s+L_{1-\rm sat})}{L_{1-\rm sat}+L_{2-\rm sat}+L_s} \tag{7}$$

where $L_{\rm air-in}$, and $L_{\rm air-out}$ are the air-core inductances measured from the inner (primary) and the outer (secondary) windings. Parameters $L_{1-\rm sat}$, and $L_{2-\rm sat}$ are the slopes of the deep saturation parts of the hysteresis branches corresponding to the primary and secondary windings. Equations (6) and (7) are solved first for $L_{2-\rm sat}$ as follows:

$$\begin{aligned} &[L_{\rm air-out}-L_{\rm air-in}-L_s]\,L_{2-\rm sat}^2 \\ &\quad + \left[2L_{\rm air-out}L_s - L_s^2\right]L_{2-\rm sat} + L_s^2 L_{\rm air-out} = 0 \end{aligned} \tag{8}$$

which is a quadratic equation with the following analytical solution:

$$\begin{aligned} L_{2-\rm sat} &= \left(\frac{L_s}{L_{\rm air-out}-L_{air-in}-L_s}\right) \\ &\quad \times \left(L_s - 2L_{\rm air-out} \pm \sqrt{L_s^2+4L_{\rm air-in}L_{\rm air-out}}\right) \end{aligned} \tag{9}$$

then parameter $L_{1-\rm sat}$ is calculated from (6) as

$$L_{1-\rm sat} = \frac{L_{\rm air-in}(L_{2-\rm sat}+L_s)}{L_{2-\rm sat}+L_s-L_{\rm air-in}}. \tag{10}$$

Equations (9) and (10) do not require an iterative process. The solution is always real, because the term under the radical sign in (9) is always positive. It can be proven that a positive value for $L_{2-\mathrm{sat}}$ is obtained if the following condition is satisfied:

$$L_{\mathrm{air-out}} < L_s + L_{\mathrm{air-in}}. \tag{11}$$

In Appendix A, it is shown that (11) is physically sound and always valid for standard single-phase transformer designs. Hysteresis curves of the two magnetizing branches are extended using $L_{1-\mathrm{sat}}$ and $L_{2-\mathrm{sat}}$ as the slopes from the last measured point to infinity. The calculated deep saturation parameter values for the model representing the innermost and the outermost windings are given in Appendix B.

D. Adaptive-Dual Model for Various Operating Conditions

The aforementioned modifications to the π model make the proposed reversible model compatible with the principle of duality in all (low-frequency) operating conditions. It unifies the electrical equivalent circuits as follows.

1) During the normal operating condition (loaded transformer), the magnetizing branches work below the saturation knee. Thus, these shunt inductors are much larger than the leakage inductance and, therefore, they are negligible. Note that in this condition that no considerable flux penetrates into the air (other than in the leakage region). Therefore, inductances representing air (L_{A1}, L_{A2}, and L_{A3}) are also negligible.
2) When the transformer is open circuited, the leakage inductance is negligible. Therefore, the two nonlinear magnetizing branches are effectively in parallel.
3) In deep saturation, all nonlinear components (iron core and air) enter the saturation region. Therefore, according to (6) and (7), the inductances seen from each terminal are the air-core inductance of the corresponding windings.

III. Simulation Results Versus Measurements

To validate the proposed model, a reversible circuit is derived for a pair of windings at a time (as a single-phase two-winding transformer). The models are tested for inrush currents, GIC, and series ferroresonance.

Among all combinations, the reversible model representing the innermost and the outermost windings is the one of greatest interest. In this case, windings are separated and leakage inductance is the maximum among all possible configurations for this transformer.

A. Inrush Currents

Maximum inrush currents occur when the transformer is energized at the zero crossing of the voltage sine wave with the secondary winding open circuited on a demagnetized core. A zero crossing switch is connected between the transformer terminals and the power source [21]. To ensure the consistency of the measurements, the transformer iron core is completely demagnetized before each experiment. The source impedance $Z_s = 0.144\ \Omega$ is measured, which is almost purely resistive. Fig. 7 illustrates the test setup for inrush current experiments.

Inrush current tests are performed from primary and secondary sides. Laboratory measurements are compared versus

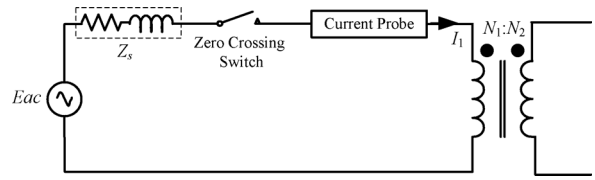

Fig. 7. Test setup for inrush current measurements.

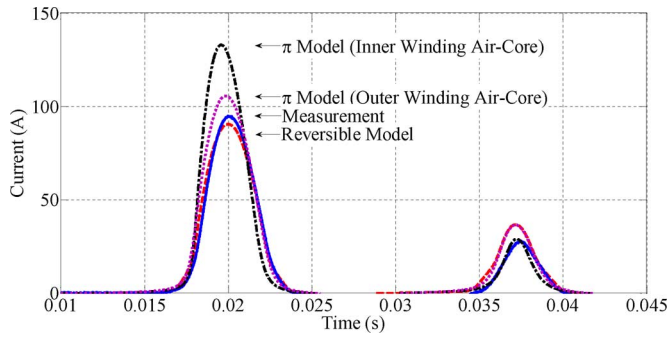

Fig. 8. Comparison between inrush currents measurements and simulations for switching on the outermost winding.

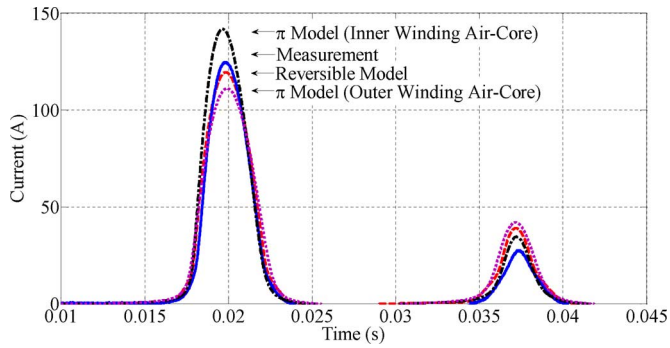

Fig. 9. Comparison between inrush currents measurements and simulations for switching on the innermost winding.

EMTP simulations in Figs. 8 and 9. In these figures, the reversible transformer model is compared against the π model and measurements for the innermost and outermost windings. Note that the π model is simulated for two conditions: 1) considering the air-core inductance seen from the innermost winding and 2) considering the air-core inductance seen from the outermost winding. The figure shows the discrepancy of the π model results with experiments when the wrong side air-core inductance is selected. For example, the π model shows 40.5% error in the maximum inrush current value when the innermost winding air-core inductance is used for the inrush current simulations of the outermost winding. Thus, to have a proper response with the π model, it is necessary to change the air-core inductance to the corresponding value of the energized winding. In contrast, the parameters of the reversible model remain unchanged. All required information to reproduce the π model simulations is available in [21].

With the proper selection of the air-core inductance, the π model shows 13.9% and 11.6% error in the maximum inrush current values for the innermost and the outermost windings, respectively. The reversible model results are very close to the measurements with acceptable engineering accuracy (differ-

TABLE I
COMPARISON OF INRUSH CURRENT PEAK VALUES FOR THE MODELS REPRESENTING EACH PAIR OF WINDINGS (AMPERES)

Windings	Tests		Model		Differences (%)	
	Inner	Outer	Inner	Outer	Inner	Outer
1,2	124.4	110.6	119.7	106.5	3.8	3.7
1,3	124.4	104.5	121.8	102.7	2.1	1.7
1,4	124.4	94.6	119.3	90.4	4.1	4.4
2,3	110.6	104.5	105.2	101.1	4.9	3.2
2,4	110.6	94.6	103.5	95.3	6.4	0.7
3,4	104.5	94.6	99.6	89.5	4.7	5.4

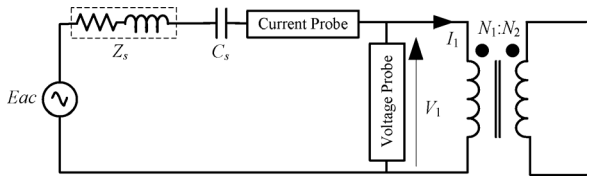

Fig. 10. Test setup for ferroresonance measurements.

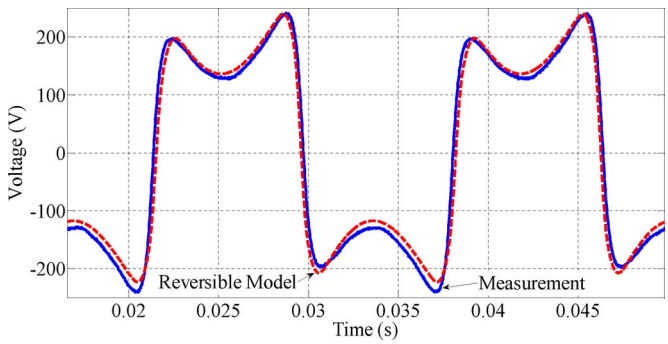

Fig. 11. Terminal voltage of the innermost winding with 60-μF series capacitance.

ences less than 5%). The relative differences of the reversible model for the outermost and the innermost windings are 4.4%, and 4.1%. An extensive comparison for the peak inrush currents obtained by simulations versus measurements is presented in Table I. One can conclude that the reversible model is very accurate. Note that the reversible model is simulated for each pair of windings as a single-phase two-winding transformer.

B. Series Ferroresonance

In this section, the reversible model is validated versus measurements for ferroresonance simulations. The schematic diagram of the experimental test setup is illustrated in Fig. 10. Note that ferroresonance has a chaotic behavior, and is very sensitive to initial conditions. In order to accurately measure voltage and current, the transformer was completely demagnetized. Also, before each experiment, it is verified that the capacitor was completely discharged [22].

The model developed for the outermost and the innermost windings is evaluated versus measurements. The primary voltage shown in Fig. 11 demonstrates ferroresonance between a 60 μF capacitance and the innermost winding. Experiments show that the π model is also capable of properly predicting the overvoltages with acceptable engineering accuracy. Therefore, the results for the π model are not presented here.

TABLE II
MAXIMUM TEMPORARY OVERVOLTAGE MEASURED VERSUS SIMULATIONS (IN VOLTS)

C_s (μF)	Test		Model		Difference (%)	
	Inner	Outer	Inner	Outer	Inner	Outer
20	204	198.2	213.2	186.2	4.5	5.9
30	214.5	207.2	221.8	197.1	3.4	4.8
60	239.9	233	239.4	223	0.2	4.3

TABLE III
PEAK VALUE OF THE TERMINAL CURRENT MEASURED VERSUS SIMULATIONS (IN AMPERES)

C_s (μF)	Test		Model		Difference (%)	
	Inner	Outer	Inner	Outer	Inner	Outer
20	8.9	8.7	9.1	9.2	2.2	5.7
30	14.4	14	13.5	13.2	6.2	5.7
60	39.9	31.4	39.3	32.6	1.5	3.8

TABLE IV
NUMERICAL VALUES OF THE MAGNETIZING CURVE MEASURED BY EXCITING THE INNERMOST WINDING

Point	I (A)	λ (Wb)	Point	I (A)	λ (Wb)	Point	I (A)	λ (Wb)
1	0.061	0	15	0.989	0.452	29	7.776	0.610
2	0.085	0.083	16	1.135	0.467	30	8.545	0.617
3	0.098	0.124	17	1.343	0.481	31	9.375	0.623
4	0.122	0.223	18	1.550	0.495	32	10.23	0.629
5	0.159	0.281	19	1.807	0.508	33	11.16	0.634
6	0.171	0.299	20	2.185	0.521	34	12.06	0.638
7	0.220	0.318	21	2.576	0.533	35	12.93	0.641
8	0.317	0.336	22	3.040	0.545	36	13.72	0.644
9	0.391	0.353	23	3.589	0.556	37	14.37	0.647
10	0.500	0.371	24	4.175	0.567	38	14.92	0.648
11	0.549	0.388	25	4.810	0.577	39	15.23	0.649
12	0.659	0.404	26	5.518	0.586	40	15.32	0.650
13	0.769	0.421	27	6.274	0.595			
14	0.891	0.436	28	6.995	0.603			

TABLE V
LAST POINT OF MAGNETIZING CURVE FOR THE MODEL REPRESENTING THE OUTERMOST AND INNERMOST WINDINGS (DEEP SATURATION)

Branch	Point	I (A)	λ (Wb)	Inductance (μH)
Left (innermost)	41	500	1.336	$L_{1\text{-}sat}$: 707.8
Right (outermost)	41	500	6.191	$L_{2\text{-}sat}$: 5716

TABLE VI
LEAKAGE INDUCTANCES BETWEEN EACH PAIR OF WINDINGS

Winding	$L_{s1,2}$	$L_{s1,3}$	$L_{s1,4}$	$L_{s2,3}$	$L_{s2,4}$	$L_{s3,4}$
Leakage (μH)	343.2	781.7	920	306.3	698.7	335

A complete comparison study is presented in Tables II and III. The numerical values are voltage and current peaks when ferroresonance occurs between the transformer and a 20-μF, 30-μF, or 60-μF capacitance, respectively. The results show satisfactory agreement between measurements and simulations with the reversible transformer model.

C. Geomagnetic Induced Currents (GICs)

Geomagnetic disturbances are capable of creating dc voltage gradients in the order of 3 to 6 V/km on the surface of the earth [25]. Thus, during GIC, power transformer neutrals are biased

TABLE VII
AIR-CORE INDUCTANCES AND RESISTANCES OF THE WINDINGS

Winding	Innermost	Inner	Outer	Outermost
Air-core Inductance (μH)	639.6	894	973	1267
ac Resistance (Ω)	0.373	0.395	0.415	0.438

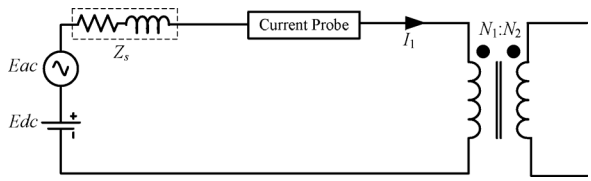

Fig. 12. Simulation setup for geomagnetic-induced currents.

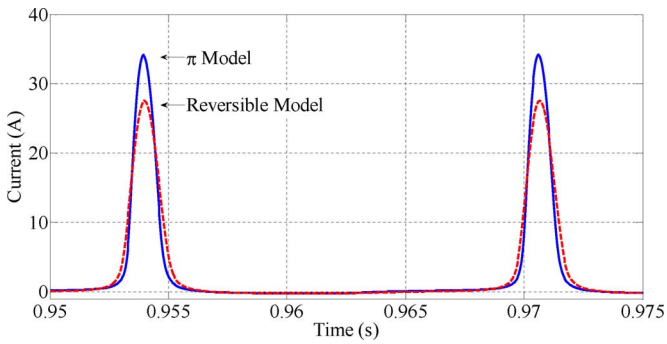

Fig. 13. Terminal currents of the outer winding during GIC.

with a dc voltage. The offset saturation condition as the results of GIC is investigated here. The phenomenon produces high amplitude currents in steady state because the core saturates. The performance of the reversible model is compared by simulation versus the π model with the circuit presented in Fig. 12.

The reversible and π models were tested for the four winding standard transformer of Fig. 1. The differences in GIC were negligible (under 10%). However, for a small leakage inductance transformer with a flat and narrow hysteresis cycle, the differences became considerable with a dc bias of 1 V. The complete data for this transformer are available in [21]. This result indicates that for large power transformers with thin hysteresis cycles, the reversible model could be more promising. The differences in peak values are 23.6% and 23.3% for the outer and the inner windings, respectively. A comparison between the terminal currents of the outer winding produced with the two models is presented in Fig. 13.

IV. DISCUSSION

In contrast with the model of [14], the model presented in this paper can be easily implemented in EMTP-type programs. All components are available in the library of the EMTP. Simple formulas are derived to efficiently calculate the parameters. The model is physically sound and in full agreement with the principle of duality. In addition, low-frequency transients were calculated with high accuracy. Thus, the principal advantages of the proposed method are simplicity and high accuracy.

The value of $L_{1-\mathrm{sat}}$, computed with (9), (10) is about 8 times the value of $L_{2-\mathrm{sat}}$ [see Fig. 6(b) and Table V]. Almost the same ratio exists between the magnetic energies of $L_{A1}+L_{A2}$ and L_{A3} computed with the finite-element simulations (see Fig. 5 when $\mu_r \rightarrow 1$). This confirms that the parameters derived by (9) and (10) correspond to a physically valid representation of the transformer components.

The model presented in this paper is only valid for single-phase two-winding transformers. However, it is believed that the same methodology can be developed for multiwinding single-phase or multiphase transformers. A general model for multiphase and/or multiwinding transformers will be presented in an upcoming paper.

V. CONCLUSION

A reversible transformer model has been developed for the calculation of low-frequency transients. The model is derived from physically consistent modifications on the conventional duality π model by recognizing that the energy in the air becomes nonlinear when the core saturates.

Step-by-step laboratory test guidelines are provided to compute the model parameters with simple formulas. The parameters can be calculated without the knowledge of geometrical information, which is hardly ever provided by the manufacturers.

The transient behavior of the reversible transformer model has been verified experimentally with inrush currents and ferroresonance measurements. The results show the superiority of the reversible model in comparison to the π model, which is known to be better than the standard T model.

APPENDIX A
PHYSICAL CONSISTENCY OF (9)

In this section, the geometrical information of the innermost (1st) and the outermost (4th) windings is used for physical validation of (9). The leakage inductance L_s and the air-core inductances (long solenoid assumption for coils) could be derived approximately from [11]

$$L_s = \frac{\mu_0 N^2 l}{h}\left[\frac{a_1}{3} + d_{14} + \frac{a_4}{3}\right] \tag{12}$$

$$L_{\mathrm{air-out}} = \frac{\mu_0 N_4^2 A_4}{h_4} = \frac{\mu_0 N_4^2 (w_4 d_4)}{h_4} \tag{13}$$

$$L_{\mathrm{air-in}} = \frac{\mu_0 N_1^2 A_1}{h_1} = \frac{\mu_0 N_1^2 (w_1 d_1)}{h_1} \tag{14}$$

where N is the common (or base) number of turns, l is the mean length of the winding turn, A is the effective area, and h is the height of the core. Parameters N_1, N_4, h_1, and h_4 are the number of turns and the height of the innermost and outermost windings, respectively. Other geometrical parameters are defined in Fig. 14. From this figure, the area can be computed as $w_4 d_4 - w_1 d_1 = l d_{14}$. Assuming $h = h_1 = h_4$ and $N = N_1 = N_4 = 1$, and starting with (11), we have

$$\begin{aligned} &L_{\mathrm{air-out}} - L_{\mathrm{air-in}} < L_s \\ &3(w_4 d_4 - w_1 d_1) < l(a_1 + 3d_{14} + a_4) \\ &3 l d_{14} < l(a_1 + 3d_{14} + a_4) \Rightarrow a_1 + a_4 > 0 \end{aligned} \tag{15}$$

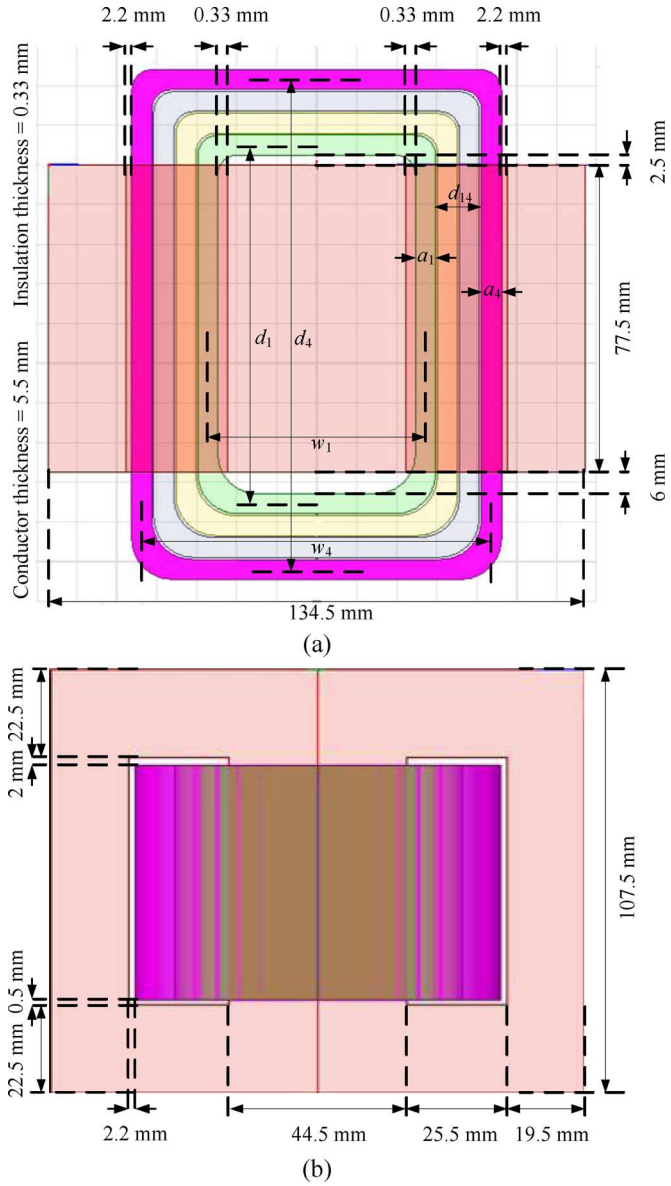

Fig. 14. Transformer dimensions: (a) top view and (b) side view.

which is always correct; therefore, $L_{1-\mathrm{sat}}$ and $L_{2-\mathrm{sat}}$ are always real and positive.

Appendix B
Transformer Information

This section provides the complete geometrical and electrical information for the transformer under study. Fig. 14 illustrates the dimensions used for finite-element simulations. Table IV presents the positive side of the iron core λ-i characteristic. The last point of the curve is obtained with the extension of numerical data presented in Table IV. The data are extended from the 40th point to infinity using $L_{1-\mathrm{sat}}$ and $L_{2-\mathrm{sat}}$ as slopes for the innermost and outermost windings, respectively. These calculated values are presented in Table V. Table VI provides the leakage inductances between different windings. Table VII includes resistance and air-core inductance values corresponding to each winding.

References

[1] J. A. Martínez and B. A. Mork, "Transformer modeling for low and mid-frequency transients—A review," *IEEE Trans. Power Del.*, vol. 20, no. 2, pt. 2, pp. 1625–1632, Apr. 2005.

[2] J. A. Martínez, R. Walling, B. Mork, J. Martin-Arnedo, and D. Durbak, "Parameter determination for modeling systems transients. Part III: Transformers," *IEEE Trans. Power Del.*, vol. 20, no. 3, pp. 2051–2062, Jul. 2005.

[3] Slow Transients Task Force of the IEEE, Modeling and Analysis of System Transients Using Digital Programs Working Group, "Modeling and analysis guidelines for slow transients—Part III: The study of ferroresonance," *IEEE Trans. Power Del.*, vol. 15, no. 1, pp. 255–265, Jan. 2000.

[4] F. de León and A. Semlyen, "Complete transformer model for electromagnetic transients," *IEEE Trans. Power Del.*, vol. 9, no. 1, pp. 231–239, Jan. 1994.

[5] A. Narang and R. H. Brierley, "Topology based magnetic model for steady-state and transient studies for three phase core type transformers," *IEEE Trans. Power Syst.*, vol. 9, no. 3, pp. 1337–1349, Aug. 1994.

[6] C. M. Arturi, "Transient simulation and analysis of a three-phase five-limb step-up transformer following and out-of-phase synchronization," *IEEE Trans. Power Del.*, vol. 6, no. 1, pp. 196–207, Jan. 1991.

[7] X. Chen and S. S. Venkata, "A three-phase three-winding core-type transformer model for low-frequency transient studies," *IEEE Trans. Power Del.*, vol. 12, no. 2, pp. 775–782, Apr. 1997.

[8] B. A. Mork, "Five-legged wound-core transformer model: Derivation, parameters, implementation, and evaluation," *IEEE Trans. Power Del.*, vol. 14, no. 4, pp. 1519–1526, Oct. 1999.

[9] B. A. Mork, F. Gonzalez, D. Ishchenko, D. L. Stuehm, and J. Mitra, "Hybrid transformer model for transient simulation—Part I: Development and parameters," *IEEE Trans. Power Del.*, vol. 22, no. 1, pp. 248–255, Jan. 2007.

[10] B. A. Mork, F. Gonzalez, D. Ishchenko, D. L. Stuehm, and J. Mitra, "Hybrid transformer model for transient simulation-part II: Laboratory measurements and benchmarking," *IEEE Trans. Power Del.*, vol. 22, no. 1, pp. 256–262, Jan. 2007.

[11] F. de León and J. A. Martinez, "Dual three-winding transformer equivalent circuit matching leakage measurements," *IEEE Trans. Power Del.*, vol. 24, no. 1, pp. 160–168, Jan. 2009.

[12] N. Chiesa, B. A. Mork, and H. K. Høidalen, "Transformer model for inrush current calculations: Simulations, measurements and sensitivity analysis," *IEEE Trans. Power Del.*, vol. 25, no. 4, pp. 2599–2608, Oct. 2010.

[13] R. Yacamini and H. Bronzeado, "Transformer inrush calculations using a coupled electromagnetic model," in *Proc. Inst. Elect. Eng., Sci. Meas. Technol.*, Nov. 1994, vol. 141, pp. 491–498.

[14] S. E. Zirka, Y. I. Moroz, C. M. Arturi, N. Chiesa, and H. K. Høidalen, "Topology-correct reversible transformer model," *IEEE Trans. Power Del.*, vol. 27, no. 4, pp. 2037–2045, Oct. 2012.

[15] J. J. Rico, E. Acha, and M. Madrigal, "The study of inrush current phenomenon using operational matrices," *IEEE Trans. Power Del.*, vol. 16, no. 3, pp. 231–237, Jul. 2001.

[16] Y. Wang, S. G. Abdulsalam, and W. Xu, "Analytical formula to estimate the maximum inrush current," *IEEE Trans. Power Del.*, vol. 23, no. 2, pp. 1266–1268, Apr. 2008.

[17] X. Wang, D. W. P. Thomas, M. Sumner, J. Paul, and S. H. L. Cabral, "Characteristic of Jiles-Atherton model parameters and their application to transformer inrush current simulation," *IEEE Trans. Magn.*, vol. 44, no. 3, pp. 340–345, Mar. 2008.

[18] E. C. Cherry, "The duality between interlinked electric and magnetic circuits and the formation of transformer equivalent circuits," in *Proc. Phys. Soc.*, Feb. 1949, vol. (B)62, pp. 101–111.

[19] A. Boyajian, "Resolution of transformer reactances into primary and secondary reactances," *AIEE Trans.*, pp. 805–810, Jun. 1925.

[20] F. de León, P. Gómez, J. A. Martinez-Velasco, and M. Rioual, "Transformers," in *Power System Transients: Parameter Determination*. Boca Raton, FL: CRC, 2009, ch. 4, pp. 177–250.

[21] F. de León, A. Farazmand, and P. Joseph, "Comparing the T and π equivalent circuits for the calculation of transformer inrush currents," *IEEE Trans. Power Del.*, vol. 27, no. 4, pp. 2390–2398, Oct. 2012.

[22] S. Jazebi, A. Farazmand, B. P. Murali, and F. de León, "A comparative study on π and T equivalent models for the analysis of transformer ferroresonance," *IEEE Trans. Power Del.*, vol. 28, no. 1, pp. 526–528, Jan. 2013.
[23] S. Jazebi, F. de León, and B. Vahidi, "Duality-synthesized circuit for eddy current effects in transformer windings," *IEEE Trans. Power Del.*, vol. 28, no. 2, pp. 1063–1072, Apr. 2013.
[24] F. de León, S. Jazebi, and A. Farazmand, "Accurate measurement of the air-core inductance of iron-core transformers with a non-ideal low-power rectifier," *IEEE Trans. Power Del.*, to be published.
[25] R. A. Walling and A. H. Khan, "Characteristics of transformer exciting current during geomagnetic disturbances," *IEEE Trans. Power Del.*, vol. 6, no. 4, pp. 1707–1714, Oct. 1991.

Saeed Jazebi (S'10) was born in 1983 in Kerman, Iran. He received the B.Sc. degree from Shahid Bahonar University, Kerman, Iran, in 2006, the M.Sc. degree in electrical engineering from Amirkabir University of Technology, Tehran, Iran, in 2008, and is currently pursuing the Ph.D. degree in electrical engineering from the Polytechnic Institute of New York University, Brooklyn, NY.

His research interests include electromagnetic design, modeling and simulation of electrical machines, and power system components, statistical pattern recognition applications in power engineering, power system protection, and power quality.

Francisco de León (S'86–M'92–SM'02) received the B.Sc. and the M.Sc. (Hons.) degrees in electrical engineering from the National Polytechnic Institute, Mexico City, Mexico, in 1983, and 1986, respectively, and the Ph.D. degree in electrical engineering from the University of Toronto, Toronto, ON, Canada, in 1992.

He has held several academic positions in Mexico and has worked for the Canadian electric industry. Currently, he is an Associate Professor at the Polytechnic Institute of New York University, Brooklyn, NY. His research interests include the analysis of power definitions under nonsinusoidal conditions, the transient and steady-state analyses of power systems, the thermal rating of cables and transformers, and the calculation of electromagnetic and thermal fields applied to machine design and modeling.

Ashkan Farazmand was born in Tehran, Iran, in 1983. He received the M.Sc. (Hons.) degree in electrical engineering from the University of Tehran, Tehran, Iran, in 2009, and the Ph.D. degree in electrical engineering from the Polytechnic Institute of New York University, Brooklyn, NY, in 2013.

His research interests are the design and analysis of transformers, electrical transients, derating of electrical machines under nonsinusoidal and unbalanced conditions, and power quality.

Digvijay Deswal was born in Haryana, India, in November 1992. He is currently pursuing the B.Tech. and M.Tech. degrees in electrical engineering at the Indian Institute of Technology (IIT) Kharagpur, West Bengal, India.

He was a summer intern at the Polytechnic Institute, New York University, in 2012. His research interests include machine drives, switched-mode power-supply design, and analysis of electrical machines.